THERMAL CONDUCTIVITY OF PHASE-CHANGE MATERIAL $CaCl_2 \cdot 6H_2O$ WITH ZnO NANOPARTICLE DOPANT BASED ON TEMPERATURE-HISTORY METHOD

I.M. SUTJAHJA[1] * , A. O. SILALAHI[1], S. WONORAHARDJO[2], D. KURNIA[1]

[1] *Dept. of Physics, Faculty of Mathematics and Natural Sciences, Institut Teknologi Bandung, Jl. Ganesha 10, Bandung, 40132, Indonesia*

[2] *Building Technology Research Division, School of Architecture, Planning and Policy Development, Institut Teknologi Bandung, Jl. Ganesha 10, Bandung, 40132, Indonesia*

Determination of thermal conductivity based on temperature history (T-history) method is low in cost and can be applied directly to some samples, as it depends only on the number of temperature sensors used in a measurement. However, very little published data has reported the solid and liquid thermal conductivities of phase-change materials (PCMs) based on this analytical method. The thermal conductivity based on T-history data is related to other thermophysical parameters of the PCM, such as the solid and liquid specific heats and the latent heat of the solid–liquid phase transition. This report analyses the solid and liquid thermal conductivities of $CaCl_2 \cdot 6H_2O$ as an inorganic PCM, using thermophysical parameters obtained from two methods of analysis, namely the T-history method proposed by Zhang et al. and its improvement by Hong et al. (Z/H) and Marin et al. (M) based on the temperature-dependent enthalpy curve. The data predict the enhancement of thermal conductivity with 1 wt.% ZnO nanoparticles as a dopant, which permit effective heat transport in the material in response to environmental heat.

Keywords: *: Phase-change material (PCM), $CaCl_2 \cdot 6H_2O$ + ZnO dopant, T-history method, solid and liquid specific heats, heat of fusion, enthalpy-temperature curve, solid and liquid thermal conductivities*

1. Introduction

Thermal energy storage (TES) based on phase-change materials (PCMs) provides better heat storage performance than common TES materials such as brick, concrete, stone, which only store sensible heat [1-3]. This is because PCMs can store and release relatively large amounts of thermal energy around their phase transition point (melting temperature for solid–liquid phase transition) in the form of both latent and sensible heat with smaller temperature variations [4,5]. The heat storage performance of a PCM is generally determined by its thermophysical parameters, including the solid and liquid specific heats and heat of fusion related to the solid–liquid phase transition. The thermal conductivity is also an important property of materials intended to conduct heat [6].

Like heat-transfer fluids, the thermophysical parameters and thermal conductivities of PCMs are generally affected by dopants of different types and concentrations. Among many commonly used dopants are mesoporous silica [7], nanoparticles of graphite, metals, and metal oxides; examples are given in [6, 8-12]. In this report, we describe the thermophysical parameters and solid and liquid thermal conductivities of the inorganic salt hydrate PCM of $CaCl_2 \cdot 6H_2O$ doped with 1 wt.% ZnO nanoparticles, determined via the T-history method first proposed by Zhang et al. [13]. This material is potentially applicable in buildings [14,15] because it has a melting temperature just above the human comfort zone, relatively large melting enthalpy, and stable phase transition [16,17]. Compared to conventional methods such as differential scanning calorimetry (DSC) or direct thermal conductivity measurements, the T-history method offers the advantages**,** of relatively low cost and good reliability because it uses relatively substantial amount of samples. Moreover, the measurement can be applied directly to some samples as it depends only on the number of temperature sensors used in a measurement. In particular for thermal conductivity, very little data has been reported in the literature, while some available data includes only the final values for some PCMs without any detailed analysis [13,18,19]. The thermal conductivity of PCM greatly affects its performance in responding to diurnal air temperature.

2.Thermophysical parameters of PCMs

The T-history method is based on the lumped capacitance method [20]. In this case, when the Biot number, defined by $Bi = hR/2\kappa$, is less than 0.1, where h is the natural convective heat-transfer coefficient, R is the tube radius, and κ is the thermal conductivity of the PCM, then the temperature distribution in the sample can be regarded as uniform.

Zhang et al. [13] proposed a method to analyse the T-history data of PCM for the

* Autor corespondent/*Corresponding author*,
E-mail: inge@fi.itb.ac.id

solidification process. This method was then improved by Hong et al. [21] to include the possibility of temperature changes of material during phase transformation and to determine the end of the phase transition process with greater accuracy. Considering these improvements, the thermophysical parameters of a PCM can be obtained by the following equations, hereafter referred to as the Z/H method:

$$c_{p,l} = \left(\frac{m_{t,w} c_{p,t} + m_w c_{p,w}}{m_p} \frac{A_1}{A_1'} \right) - \frac{m_{t,p}}{m_p} c_{p,t} \quad (1)$$

$$c_{p,s} = \left(\frac{m_{t,w} c_{p,t} + m_w c_{p,w}}{m_p} \frac{A_3}{A_3'} \right) - \frac{m_{t,p}}{m_p} c_{p,t} \quad (2)$$

$$\Delta h = \left(\frac{m_{t,w} c_{p,t} + m_w c_{p,w}}{m_p} \frac{A_2}{A_2'} (T_m - T_i) \right) - \left(\frac{m_{t,p}}{m_p} c_{p,t} + \frac{c_{p,l} + c_{p,s}}{2} \right) (T_m - T_i) \quad (3)$$

In the above equations, m_p, m_w and $m_{t,p}$, $m_{t,w}$ are the masses of the PCM, water, and the tubes used for PCM and water; $c_{p,w}$ is the specific heat of water; and $c_{p,t}$ is the specific heat of the tube material. The supercooling temperature and solidification temperature are each denoted by T_s and T_m, while T_i is the inflection temperature determined as the inflection point in the temperature derivative curve. In addition, the set values of $\{A_1, A_2, A_3\}$ and $\{A_1', A_2', A_3'\}$ correspond to the area calculations below the temperature curves of PCM and water toward the air environment. Each of them signifies the sensible liquid, liquid to solid, and sensible solid phases of PCM and its corresponding to sensible liquid for water.

The temperature-dependent enthalpy can also be determined via a method proposed by Marín et al. [22], hereafter called the M method. Hence, the evaluation of the energy absorption/release of PCM in the small interval $\Delta T_j = T_{j+1} - T_j$ corresponding to the time interval $\Delta t_j = t_{j+1} - t_j$ yields the specific enthalpy change of

$$\Delta h(T_j) = \left(\frac{m_t c_{p,t} + m_w c_{p,w}}{m_p} \right) \frac{A_j}{A_j'} \Delta T_j' + \frac{m_t}{m_p} c_{p,t} \Delta T_j \quad (4)$$

In this formula, $A_j = \int_{t_j}^{t_j + \Delta t_j} (T - T_a) dt$ and $A_j' = \int_{t_j'}^{t_j' + \Delta t_j'} (T' - T_a) dt$ are the corresponding areas for PCM and water above the air environment temperature. Finally, the temperature-dependent specific enthalpy of the PCM is obtained as

$$h(T) = \sum_{i=1}^{N} \Delta h(T_j) + h_0 \quad (5)$$

where h_0 is a constant value of enthalpy, chosen by a criterion defining the enthalpy at the lowest temperature of measurement as zero. Taking the temperature derivative, the $h(T)$ curve reveals the solid and liquid specific heats as constant values at low ($T < T_k$) and high ($T > T_i$) temperatures [23].

3.Thermal Conductivity of PCM

If the test tube containing molten PCM is suddenly put into the cool water with a temperature lower than the melting temperature of PCM, solidification can be initiated. If the ratio of height to diameter of the tube is larger than 15 as pointed out by Zhang et al. [13] then the heat transfer from the PCM to water during solidification is approximately one-dimensional (1D). Hence the 1D transient heat diffusion equation for a cylindrical geometry can be written as [12]:

$$\frac{\kappa_s}{\rho_s c_{p,s}} \frac{1}{r} \frac{\partial}{\partial r} \left(r \frac{\partial T(r,t)}{\partial r} \right) = \frac{\partial T(r,t)}{\partial t}$$
$$(r_{\text{int}} < r < R,\ t > 0)$$

where κ_s is the solid thermal conductivity, ρ_s is the solid density, $c_{p,s}$ is the solid specific heat of PCM; and $T(r,t)$ is the temperature of the PCM at radius r and time t. The initial and boundary conditions are

$$T_{(r_{\text{int}}=R)} \cong T_m \quad ; \quad t = 0$$

$$\kappa_s \left. \frac{\partial T}{\partial r} \right|_{r=r_i} = h_w (T_w - T) \quad ; \quad t > 0$$

where T_m is the melting temperature of PCM, r_{int} is the radius of the interface between the solid and liquid phases of the PCM, R is the radius of the tube, and h_w is the coefficient for convective heat transfer from the tube to the stirred cool water.

At any time, the conditions for the solid/liquid interface are (Fig. 1)

$$T_{(r=r_{\text{int}})} = T_m$$

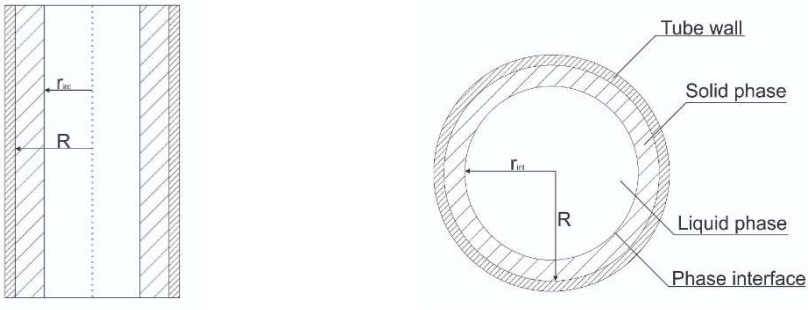

(a) (b)

Fig. 1 - (a) Front elevation and (b) cross-section of PCM in the tube during liquid-to-solid phase change, showing the coexistence of two phases with phase boundary. Adaptation from [13].

$$\frac{\kappa_s}{\rho_s h_m}\frac{\partial T}{\partial r}\bigg|_{r=r_{\text{int}}} = \frac{\partial r_{\text{int}}}{\partial t}$$

where h_m is the heat of fusion of the PCM. Using the perturbation method, by neglecting the second-order term of the perturbation expansion, the effective thermal conductivity of PCM in the solid state can be expressed as

$$\kappa_s = \frac{[1+\text{Ste}]}{4\left[\dfrac{t_f(T_m - T_w)}{\rho_s R^2 h_m} - \dfrac{1}{h_w R}\right]} \qquad (6)$$

where t_f is the time taken for complete solidification and the Stefan number is defined as $\text{Ste} = c_{p,s}(T_m - T_w)/h_m$. To simplify the formula, we may neglect the second term in the denominator, as is valid for most experiments [13], so that the formula becomes

$$\kappa_s = \frac{[1+\text{Ste}]}{4\left[\dfrac{t_f(T_m - T_w)}{\rho_s R^2 h_m}\right]} \qquad (7)$$

Similarly, if the tube containing the solid PCM is dipped into a hot water bath, which is at a temperature somewhat higher than T_m, the expression for the effective thermal conductivity of PCM in the liquid state can be achieved by following a similar procedure to that described above once the time needed for complete melting (t_m) is known:

$$\kappa_l = \frac{[1+\text{Ste}]}{4\left[\dfrac{t_m(T_w - T_m)}{\rho_l R^2 h_m}\right]} \qquad (8)$$

where $\text{Ste} = c_{p,l}(T_w - T_m)/h_m$, $c_{p,l}$ is the liquid specific heat, and ρ_l is the liquid density of the PCM. We note that equations (6), (7) and (8) are valid for Ste <0.5.

4.Method

$CaCl_2{\cdot}6H_2O$ as the PCM and a microparticulate powder of ZnO as a chemical dopant were purchased from Sigma Aldrich. Nanoparticulate ZnO with the average diameter of ~100 nm was obtained after milling the material, as described previously [24]. ZnO with 1 wt.% was added directly to $CaCl_2{\cdot}6H_2O$ and stirred by a magnetic stirrer and an ultrasonic bath to form a stable suspension. To characterise the samples by this method, the reference sample (water), $CaCl_2{\cdot}6H_2O$, and $CaCl_2{\cdot}6H_2O$ +ZnO (1 wt.%) were placed in 250-mm-long glass test tubes with 10-mm internal diameters and 1-mm-thick walls. These tube dimensions were selected to ensure that the Biot number less than 0.1 and the heat transfer occurred one-dimensionally along the length of the tube.

The setup for measurement by the T-history method is depicted in Figure 2. For the first measurement to determine the solid and liquid specific heats, heat of fusion and enthalpy, the tubes were exposed to a cool environment (T_a) provided by a cooling bath. For the second measurement to determine the solid and liquid thermal conductivities, the tubes were dipped into cool and warm water environments (T_w). Both the air and water environments are controlled by a temperature controller. Each tube is equipped with temperature sensors (T-type thermocouples of ~1 mm in diameter) that are integrated to the data logger (Applent AT4508A from Applent Instruments, Inc.) and a computer.

Before the first measurement, the water and liquid PCMs contained in different tubes were heated to a certain high temperature ($T_{0,a}$) above the melting point (T_m) and stabilised for a few minutes to ensure homogeneity of temperature throughout the samples. The tubes were then exposed to a cool environment (T_a). During the cooling process the temperatures of the water and PCM were recorded and plotted versus time until the PCMs solidified.

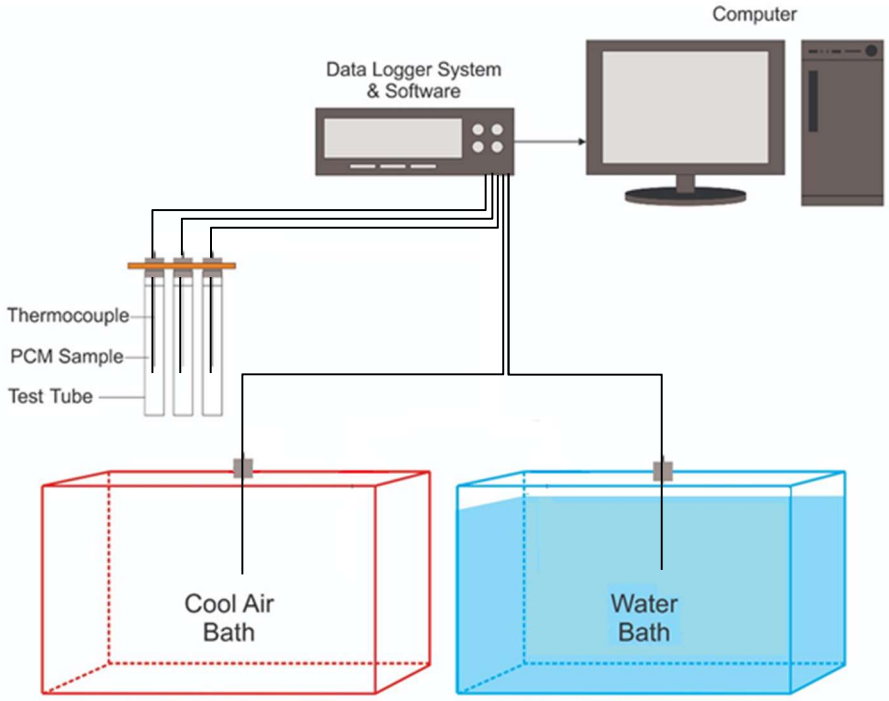

Fig. 2 - Schematic of the T-history method used to measure the thermophysical parameters of PCM. For solid/liquid specific heats and heat of fusion/enthalpy measurements, the tubes were exposed to a cool air environment (T_a) provided by a cooling bath. For solid and liquid thermal conductivities measurements, the tubes were dipped into cool and warm water environments (T_w).

For the second measurement, the tubes were dipped into a cool water environment (T_w) to determine the solid thermal conductivity (κ_s) and a warm water environment (T_w) for the liquid thermal conductivity (κ_l). Before κ_s measurement, the liquid PCMs contained in different tubes were heated to a certain high temperature ($T_{0,w}$) above the melting point (T_m) and stabilised for a few minutes to ensure temperature homogeneity. The tubes were then subsequently exposed to a cool water environment (T_w), and during the cooling process, the temperatures of the PCMs were recorded until the PCMs solidified. On the other hand, prior to κ_l measurement, the solid PCMs contained in different tubes were cooled to a certain low temperature ($T_{0,w}$) well below the melting point (T_m). The tubes were then subsequently exposed to a warm water environment (T_w) with the temperature well above T_m, and during the melting process, the temperatures of the PCMs were recorded until the PCMs melted. The overall experiments were repeated four times to ensure the accuracy and reproducibility of the data.

The densities of $CaCl_2{\cdot}6H_2O$ and $CaCl_2{\cdot}6H_2O$ + ZnO (1 wt.%) were measured by using a pycnometer. The result for pure $CaCl_2{\cdot}6H_2O$ showed a good agreement with the data from references [6,14], with the difference between solid and liquid densities of ~9%. The density increases about 0.7% with the ZnO dopant concentration because the molar mass of ZnO is higher than that of $CaCl_2{\cdot}6H_2O$.

5.Results and Discussion

5.1.Thermophysical parameters of $CaCl_2{\cdot}6H_2O$ and their variations with ZnO dopant

The typical T-history data of $CaCl_2{\cdot}6H_2O$ and $CaCl_2{\cdot}6H_2O$+ ZnO (1 wt.%) during the heat release of the solidification process in air are shown in Fig. 3.

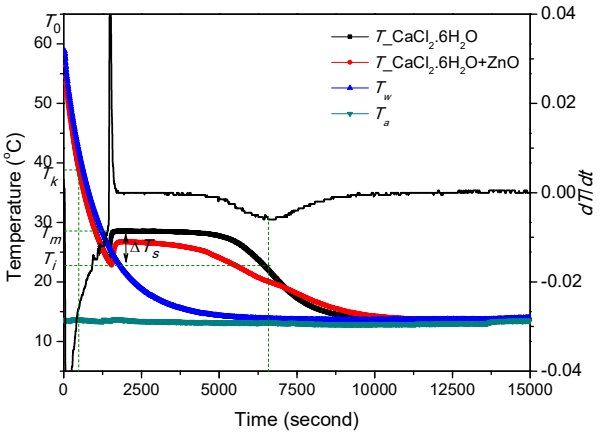

Fig. 3 - Typical T-history data of $CaCl_2{\cdot}6H_2O$ and $CaCl_2{\cdot}6H_2O$ + ZnO in air environment with water as reference material, and their derivative curve (for clarity, the derivative curve is only shown for $CaCl_2{\cdot}6H_2O$). T_0, T_s (not shown), and T_m in the *T-t* curve signify the initial, supercooling, and solidification temperatures, and ΔT_s is the supercooling degree. T_i and T_k signify the inflection and kink temperatures in the temperature derivative curves, indicating the phase transition region.

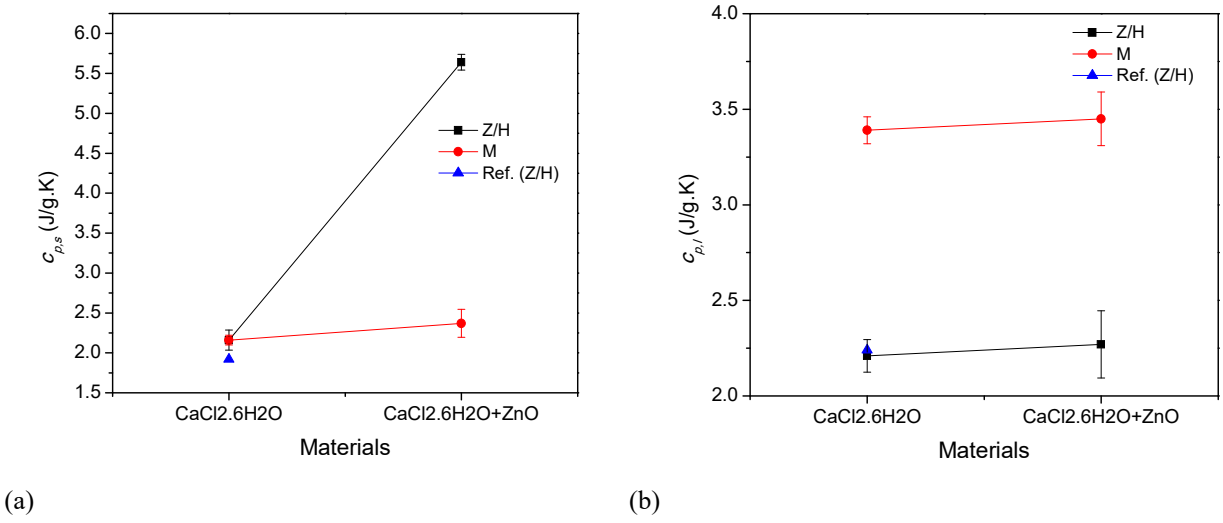

(a) (b)

Fig. 4 - The average and error values of (a) solid and (b) liquid specific heats of $CaCl_2 \cdot 6H_2O$ and $CaCl_2 \cdot 6H_2O$ + ZnO dopant, as derived from Z/H method (black rectangles) and M method (red circles). Shown also in the graph the data from the reference [9].

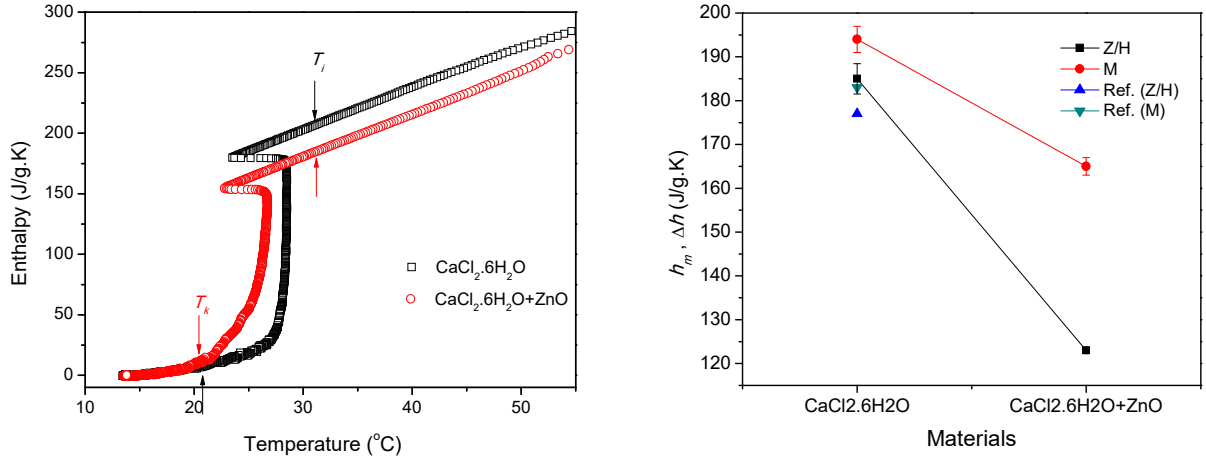

(a) (b)

Fig. 5 - (a) The typical enthalpy–temperature curve of $CaCl_2 \cdot 6H_2O$ and $CaCl_2 \cdot 6H_2O$ + ZnO dopant derived from the M method. (b) The average and error values of the heats of fusion (black rectangles) and enthalpy jumps (red circles) derived from $h(T)$ curved between T_i and T_k. Shown also in the graph the data from the reference [9].

From this Figure, it is seen that $CaCl_2 \cdot 6H_2O$ undergoes a clear phase transition at a sharp temperature, corresponding to the melting temperature (T_m). This transition becomes gradual with 1 wt. % ZnO dopant addition. The melting (T_m) and supercooling (T_s) temperatures are decreased with 1 wt. % ZnO doping, leading to a reduction of supercooling degree (ΔT_s) as measured by the difference between T_m and T_s. Plotted also in Fig. 1 are the temperature derivatives of the T-history data, which show two other important temperature characteristics, namely the kink (T_k) and inflection (T_i) temperatures; these signify the beginning and end of the latent-heat release process [23].

From the data in Fig. 3, the thermophysical parameters are analysed by means of the Z/H and M methods to reveal the temperature dependent enthalpy curve, $h(T)$. The results are shown in Fig. 4 for solid ($c_{p,s}$) and liquid ($c_{p,l}$) specific heats and Fig. 5 for $h(T)$ curve, the heat of fusion h_m, and enthalpy jump Δh. We note that Δh is determined as the difference of enthalpy values between T_i and T_k in the $h(T)$ curve. Moreover, constant values of $c_{p,s}$ and $c_{p,l}$ based on M method are obtained by taking the temperature derivative of the $h(T)$ curve at low ($T < T_k$) and high ($T > T_i$) temperatures. For each graph, we shown also the related average data from reference [9].

In figures 4 and 5, the values of $c_{p,s}$, $c_{p,l}$ and h_m or Δh are close to the reference values [9] based on the same method. Comparing the $c_{p,s}$ and $c_{p,l}$ values obtained from the two different methods (Z/H and M), it can be seen from Fig. 4 that the specific heats generally tend to increase with dopant addition. A very good agreement is found for the $c_{p,s}$ value of pure $CaCl_2 \cdot 6H_2O$, while a large increase is found for the 1 wt. % ZnO-doped material via the data analysis following the Z/H method. It is interesting that the same slope of increase is found for $c_{p,l}$, while the values obtained from the M method are larger than those obtained from the Z/H method. Moreover, the enthalpy jump or heat of fusion related to the latent heat storage capacity is decreased with the dopant, with almost equal behaviours between the Z/H and M methods. Compared to other dopant types (graphite and CuO) [9], the decrease of enthalpy is more pronounced for this 1 wt. % ZnO-doped material. In the following section, the $c_{p,s}$, $c_{p,l}$, and h_m or Δh values from the two different analysis methods are used to calculate the solid and liquid thermal conductivities of $CaCl_2 \cdot 6H_2O$ and their variations with the 1 wt. % ZnO dopant.

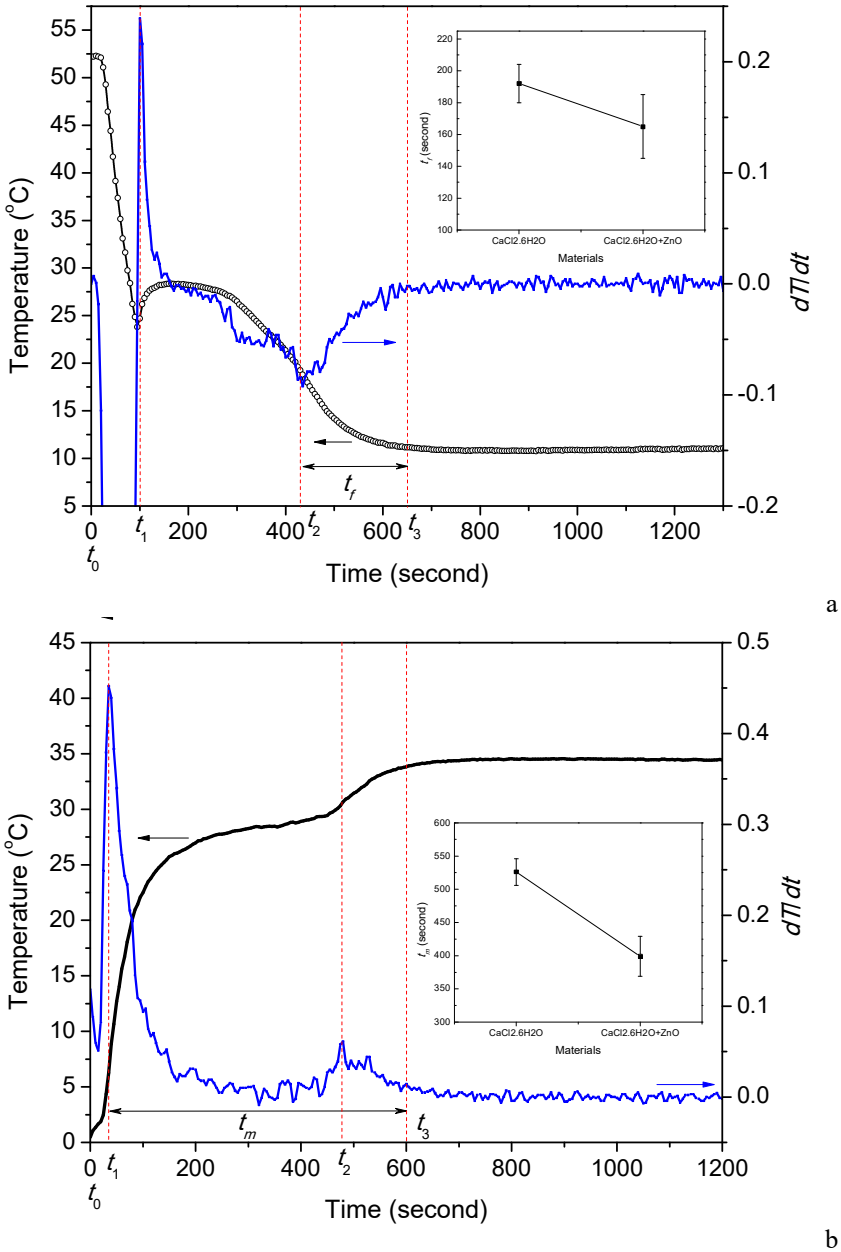

Fig. 6 - Typical T-history data of $CaCl_2 \cdot 6H_2O$ and $CaCl_2 \cdot 6H_2O$ + ZnO dopant in (a) cool water and (b) warm water to derive solid and liquid thermal conductivities. Each time-dependent temperature curve is plotted along with its derivative (dT/dt-t) curve to derive the t_m and t_f values. The insets show the dopant dependence of the t_m and t_f values.

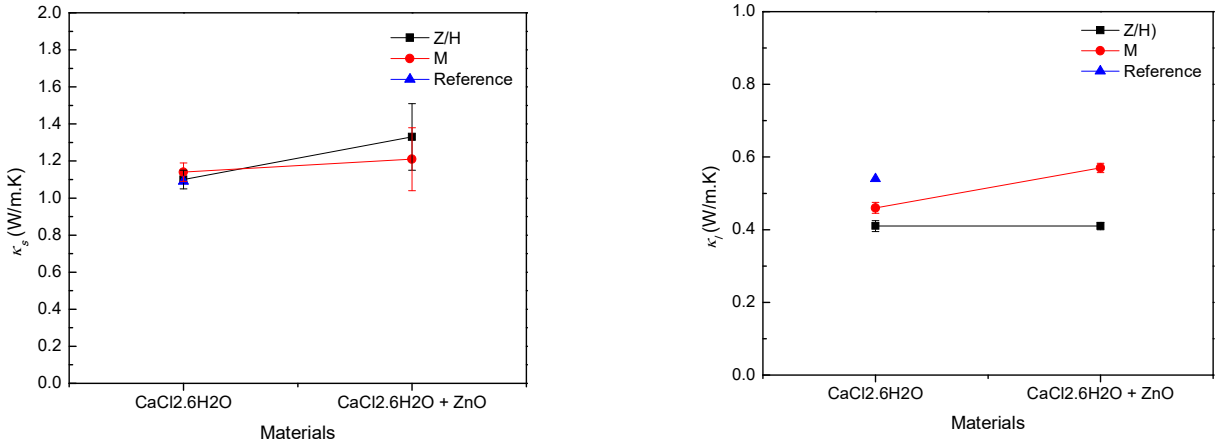

(a) (b)

Fig. 7 - The average values of (a) solid and (b) liquid thermal conductivities of $CaCl_2 \cdot 6H_2O$ and their variations with ZnO dopant inclusion. Each parameter of κ_s and κ_l is calculated by using the other thermophysical parameter values ($c_{p,s}$, $c_{p,l}$, h_m, or Δh) from the two different methods of Z/H (black squares) and M (red circles). Shown also in the graphs the data for $CaCl_2 \cdot 6H_2O$ from the references.

5.2.Thermal Conductivity

Typical experimental data for the solid and liquid thermal conductivities of $CaCl_2 \cdot 6H_2O$ and $CaCl_2 \cdot 6H_2O$ + ZnO (1 wt.%) dopant are shown in Fig. 6, along with their temperature derivative curves. From this figure, the solidification curves show similarity for the experiments performed in air (Fig. 3) and water (Fig. 6(a)), although the process in water occurs over a relatively shorter time. Thus, following Zhang [13] and Peck [25], the time boundaries for the data experiment are denoted as t_1, t_2, and t_3. Beginning from initial temperature $T_{0,w}$, the solidification process involves a sensible liquid phase at the time interval of 0–t_1, the liquid-to-solid phase transition at the time interval of t_1–t_2, and a sensible solid phase at the time interval of t_2–t_3 (Fig. 6(a)). Meanwhile, the melting process includes a sensible solid phase at the time interval of 0–t_1, the solid-to-liquid phase transition at the time interval of t_1–t_2, and a sensible liquid phase at the time interval of t_2–t_3, as shown in Fig. 6(b).

To determine the solid and liquid thermal conductivities by means of Eqs. (7) and (8), we must determine the time for complete solidification (t_f) and that for complete melting (t_m). As illustrated in Fig. 6(a), t_f is determined as the time interval between t_2 and t_3 when the material becomes a sensible solid phase, while t_m is determined as the time interval between t_1 and t_3 when the material experiences the solid-to-liquid phase change until it becomes liquid. Further analysis of the data has yielded the solid (κ_s) and liquid (κ_l) thermal conductivities shown in Fig. 7 It is notable that using thermophysical parameter values from different methods yields different exact values of κ_s and κ_l, and their variation with the dopant must also be considered.

For pure $CaCl_2 \cdot 6H_2O$, it is found that κ_s is larger than κ_l, in good agreement with direct measurements from the references, namely κ_s = 1.09 W/m·K and κ_l = 0.54 W/m·K [6, 26, 27]. Compared to these reference data, the difference in exact values is about 1–5% for κ_s and 7–15 % for κ_l. Good agreement of κ_s values is found for the thermophysical parameter values obtained from the two different data analyses (Z/H and M), and the solid thermal conductivity tends to increase with 1 wt. % ZnO dopant addition with the percentage increase of 6-20%. The κ_l values, on the other hand, show significantly different values when using the thermophysical parameters values derived from the Z/H versus M methods, with a constant value upon 1 wt. % ZnO dopant addition for Z/H method and an increase (about 24%) for M method. The relatively larger increase of κ_l with 1 wt. % ZnO dopant for the thermophysical parameter values obtained from the M method should be clarified by direct thermal conductivity measurement. We note that the enhancement of solid and liquid thermal conductivities of PCM (a mixture of hydrated salts, additives and nucleating agents) with copper dopant concentration have been reported by Jegadheeswaran et al. [18], with the superiority of microparticles compared to nanoparticles in terms of solidification and melting rates, exergy performance, and heat transfer enhancement could be further investigated in more detail.

6.Conclusion

We have described in this study the role of 1 wt. % ZnO dopant in affecting the thermophy sical parameters of the PCM $CaCl_2 \cdot 6H_2O$ by means of the T-history method. The parameters consist of the solid and liquid specific heats ($c_{p,s}$ and $c_{p,l}$) and the heat of fusion (h_m), obtained by analysing the data

through the method proposed by Zhang and Hong. In addition, the temperature-dependent enthalpy curve, $h(T)$, is obtained by the method proposed by Marin et al., and further analysis of $h(T)$ reveals the $c_{p,s}$, $c_{p,l}$ and Δh. It is found that the two methods show the same variations of the parameter values with 1 wt. % ZnO doping. In addition, the solid thermal conductivities of pure $CaCl_2{\cdot}6H_2O$ calculated by using the parameter values from Z/H and M methods show almost the same values, with relatively small error values (1–5%), compared to the directly measured value from the literature. Overall, the solid and liquid thermal conductivities tend to increase with 1 wt. % ZnO dopant addition. Lastly, the thermal conductivity based on T-history data should provide reliable data that can be used to determine the solid and liquid thermal conductivities of any PCM with dopants, in order to increase the heat exchange between the PCM and its environment. Optimising the thermal conductivity of PCMs is necessary to reduce the time delay of PCMs in responding to diurnal temperature changes and thus optimise their effectiveness in application performance.

Acknowledgement

This research is funded by Desentralisasi ITB PUPT RistekDIKTI Indonesia 2017 research program under contract number: 009/SP2H/LT/DRPM/IV/2017.

REFERENCES

1. I. Dincer, M. Rosen, Energy Storage System and Applications (John Wiley and Sons, Ltd., Ontario, Canada, 2010).
2. L. F. Cabeza (Editor), Advances in Thermal Energy Storage Systems, Methods and Applications (Woodhead Publishing, Cambridge, UK, 2015).
3. A. S. Fleischer, Thermal Energy Storage Using Phase Change Materials Fundamentals and Applications (Springer, 2015).
4. M. M. Farid, A. M. Khudhair, S. A. K. Razack, S. A. Hallaj, A review on phase change energy storage: materials and applications, Energy Conversion and Management 2004, **45**, 1597–1615.
5. A. Sharma, V. V. Tyagi, C. R. Chen, D. Buddhi, Review on thermal energy storage with phase change materials and applications, Renewable and Sustainable Energy Reviews, 2009, **13**, 318–345.
6. H. Mehling, L. Cabeza, Heat and Cold Storage with PCM (Springer, Berlin, Germany, 2008).
7. R. A. Mitran, D. Berger, C. Matei, Improving thermal properties of shape-stabilized phase change materials containing lauric acid and mesocellular foam silica by assessing thermodynamic properties of the nonmelting layer, Thermocimica Acta, 2018, **660**, 70–76.
8. T. T. Ping, Y. C. Chieh, Characteristics of phase-change materials containing oxide nano-additives for thermal storage Nanoscale Research Letters, 2012, **7**, 611.
9. I. M. Sutjahja, A. O. Silalahi, N. Sukmawati, D. Kurnia, S. Wonorahardjo, Variation of thermophysical parameters of PCM $CaCl_2.6H_2O$ with dopant from T-history data analysis, Mater. Res. Express, 2018, **5**, 034007.
10. S. Wi, J. Seo, S. G. Jeong, S. J. Chang, Y. Kang, S. Kim, Thermal properties of shape-stabilized phase change materials using fatty acid ester and exfoliated graphite nanoplatelets for saving energy in buildings, Solar Energy Materials & Solar Cells, 2015, **143**, 168–173.
11. S. Sharma, L. Micheli, W. Chang, A. A. Tahir, K. S. Reddy, T. K. Mallick, Nano-enhanced Phase Change Material for thermal management of BICPV, Applied Energy, 2017, **208**, 719–733.
12. C. Kaviarasu, D. Prakash, Review on Phase Change Materials with Nanoparticle in Engineering Applications, Journal of Engineering Science and Technology Review, 2016, **9**(4), 26- 36.
13. Y. Zhang, Y. Jiang, Y. Jiang, A simple method, the T–History method, of determining the heat of fusion, specific heat and thermal conductivity of phase-change materials, Measurement Science and Technology 1999, **10**, 201–205.
14. G. A. Lane, Low temperature heat storage with phase change materials, International Journal of Ambient Energy, 1980, **1**(3), 155–68.
15. Y. Zhang, G. Zhou, K. Lin, Q. Zhang, H. Di, Application of latent heat thermal energy storage in buildings: State-of-the-art and outlook, Building and Environment 2007, **42**, 2197–209.
16. M. Kenisarin, K. Mahkamov, Salt hydrates as latent heat storage materials: Thermophysical properties and costs, Solar Energy Materials & Solar Cells 2016, **145**, 255–286.
17. V. V. Tyagi, D. Buddhi, Thermal cycle testing of calcium chloride hexahydrate as a possible PCM for latent heat storage, Solar Energy Materials & Solar Cells, 2008, **92**(8), 891-899.
18. S. Jegadheeswaran, S. D. Pohekar, T. Kousksou, Investigations on thermal storage systems containing micron-sized conducting particles dispersed in phase change material, Matter Renew. Sustain Energy, 2012, **1**(5), 1-16.
19. X. Wang, M. Dennis, Characterisation of thermal properties and charging performance of semi-clathrate hydrates for cold storage applications, Applied Energy, 2016, **167**, 59–69.
20. T. L. Bergman, A. S. Lavine, F. P. Incropera, D. P. Dewitt, Fundamentals of Heat and Mass Transfer, 7th edition (Wiley, New York, NY, 2011).
21. H. Hong, S. K. Kim, Y. Kim, Accuracy improvement of T-history method for measuring heat of fusion of various materials, International Journal of Refrigeration, 2004, **27**, 360–366.
22. J. M. Marín, B. Zalba, L. F. Cabeza, H. Mehling, Determination of enthalpy–temperature curves of phase change materials with the temperature-history method: improvement to temperature dependent properties, Measurement Science and Technology, 2003, **14**, 184–189.
23. I. M. Sutjahja, A. O. Silalahi, D. Kurnia, S. Wonorahardjo, Thermophysical Parameters and Enthalpy-Temperature Curve of Phase-Change Material with Supercooling from T-history Data, U.P.B. Sci. Bull., Series B, 2018, **80**(2), 57-70.
24. I. M. Sutjahja, A. O. Silalahi, D. Kurnia, S. Wonorahardjo, The role of particle dopant to the thermal conductivities of PCM coconut oil by means of T-history method, Presented at 7th Asian Physics Symp. 2017—Bandung (29–31 August 2017).
25. J. H. Peck, J. J. Kim, C. Kang, H. Hong, A study of accurate latent heat measurement for a PCM with a low melting temperature using T-history method, International Journal of Refrigeration, 2006, **29**, 1225-1232.
26. V. V. Tyagi, S. C. Kaushik, A. K. Pandey, S. K. Tyagi, Experimental study of supercooling and PH behavior of a typical phase change material for thermal energy storage, Indian Journal of Pure and Applied Physics, 2011, **49**, 117-125.
27. R. Nikolić, J. Tripković, Measurements of thermal conductivities of some low melting materials in a concentric cylinder apparatus, Appl. Phys. A, 1987, **44(4)**, 293–297.

****